Catalysis Communications 156 (2021) 106321

Contents lists available at ScienceDirect

Catalysis Communications

journal homepage: www.elsevier.com/locate/catcom

Short communication

Synergistical photo-thermal-catalysis of Zn_2GeO_4:xFe^{3+} for H_2 evolution in $NaBH_4$ hydrolysis reaction

Qiaoqi Li [a,*], Fei Wang [a], Xin Zhou [a], Jianmei Chen [a,b], Chao Tang [a], Lili Zhang [a,*]

[a] School of Chemistry and Chemical Engineering, Huaiyin Normal University, Jiangsu Key Lab for Chemistry of Low-Dimensional Materials, No.111 West Changjiang Road, Huai'an 223300, Jiangsu Province, PR China

[b] College of Chemistry and Chemical Engineering, Changzhou University, Gehu Road 1, Changzhou, Jiangsu 213164, PR China

ARTICLE INFO

Keywords:
Zn_2GeO_4
$NaBH_4$ hydrolysis reaction
Hydrogen evolution
Photo-thermal-catalysis
Synergism

ABSTRACT

Herein, we reported the systematic investigation of synergistic photo-thermal-catalysis for $NaBH_4$ hydrolysis reaction based on zinc orthogermanate. A series of Zn_2GeO_4:xFe^{3+} (x = 0 to 0.10) catalysts were prepared via solvothermal method. The H_2 evolution experiments demonstrated that the photogenerated holes trap OH^- not only shifted the equilibrium of $NaBH_4$ hydrolysis reaction toward the direction of H_2 evolution, but also inhibited the recombination of photogenerated carriers. With the remarkable photo-thermal synergism for the as-prepared catalysts, the H_2 evolution rate in photo-thermal-driven condition had witnessed several times higher than that in mono-energy driven condition. The catalysts remained stable after circulation tests.

1. Introduction

Hydrogen, a fantastic clean energy carrier with high energy density (1.42×10^8 J·Kg^{-1}) is the viable alternative energy source of fossil fuels [1]. Currently, the solutions of hydrogen storage are achieved by gas compression and gas liquefaction. For the low density of hydrogen gas (0.0899 g·L^{-1}), storing compressed hydrogen requires high pressure and huge storage capacity vessel [2]. Moreover, as the low boiling point of hydrogen (20.37 K), the liquefaction and storage processes consume massive energy to maintain the low temperature environment [3]. The hydrogen storage techniques mentioned above not only uneconomic, but also with potential safety hazard in the processes of production, transportation and application. However, chemical hydrides could perfectly solve the challenges above and have been regarded as the ideal hydrogen storage medium [4].

Compared with other chemical hydrides, $NaBH_4$ is an effective and safe solid-state hydrogen resource medium with the following advantages, such as non-toxic, non-combustible, non-explosive and high hydrogen storage capacity [5]. Four moles of hydrogen can be obtained from hydrolyzing every mole of $NaBH_4$ by the following equation [6].

$$NaBH_4 + 2H_2O \rightarrow NaBO_2 + 4H_2\uparrow \left(\Delta H = -217\ \text{kJ·mol}^{-1}\right)$$

As the reaction product ($NaBO_2$) can be converted back to $NaBH_4$, it is easy to accomplish a closed-loop hydrogen energy system. During the recent decades, various of efficient catalysts have been developed for achieving rapid H_2 evolution from $NaBH_4$ hydrolysis reaction [7–10]. The first-generation catalysts were traditional noble metal-based materials, including platinum [11], silver [12], palladium [13], gold [14], rhodium [15] and ruthenium [16]. Later on, next-generation catalysts were based on the non-noble transition metal, such as ferrum [17], cobalt [18], nickel [19] and copper [20]. The catalysts exhibited excellent catalytic capacity for H_2 evolution in $NaBH_4$ hydrolysis reaction. Notably, the content of OH^- in the solution system was remarkable increased with the catalytic reaction proceeded. As a result, resulting high pH-value inhibited the hydrolysis of $NaBH_4$ solution and decreased the H_2 evolution rate [21]. The mainstream research on $NaBH_4$ hydrolysis reaction was traditional chemical catalysis driven by thermal radiation. Unlike the mechanism of traditional chemical catalysis, photocatalytic reactions based on the electron and hole pairs (e^-/h^+ pairs) generated by irradiation. Over the past several years new ideas have surged in adoption and brought about improved ways to enhance the hydrogen evolution via photocatalytic reactions [22–24]. Here, the photogenerated holes could effectively consume the excess OH^- ions, which transfer the $NaBH_4$ hydrolysis reaction equilibrium to the direction of H_2 evolution. In addition, the recombination of photogenerated e^-/h^+ pairs could effectively prevent by the consumption of photogenerated holes. Combined with the two factors above, hydrogen could be generated rapidly from $NaBH_4$ hydrolysis reaction by synergistically

* Corresponding authors.
E-mail addresses: lqq@hytc.edu.cn (Q. Li), zll@hytc.edu.cn (L. Zhang).

https://doi.org/10.1016/j.catcom.2021.106321
Received 21 March 2021; Received in revised form 18 April 2021; Accepted 1 May 2021
Available online 3 May 2021

photo-thermal-catalytic effect.

Here, the work was concerned with applying photocatalyst to $NaBH_4$ hydrolysis reaction. Zn_2GeO_4, an excellent photocatalyst was selected for the potential material as the high chemical stability. Moreover, the electronic configuration of Zn_2GeO_4 allowed excellent mobility for the photogenerated electron-hole pairs [25]. A series of Zn_2GeO_4:***x***Fe^{3+} (***x*** = 0 to 0.10) solid-solutions were obtain via a simple solvothermal method. Compared with mono-energy driven condition, the H_2 evolution rate for Zn_2GeO_4:***x***Fe^{3+} (x = 0 to 0.05) solid-solutions in photo-thermal-driven condition could be improved for several times. It was verified to certain that the synergistically photo-thermo-catalytic effect of Zn_2GeO_4 for H_2 evolution in $NaBH_4$ hydrolysis reaction. As the representative samples, Zn_2GeO_4 afforded the H_2 evolution rate of 5.45 $mmol{\cdot}h^{-1}{\cdot}g^{-1}$ under UV-light irradiation at 40 °C. Besides, Zn_2GeO_4:$0.05Fe^{3+}$ exhibited the H_2 evolution rate of 2.93 $mmol{\cdot}h^{-1}{\cdot}g^{-1}$ at 40 °C under visible-light irradiation. This work demonstrated that $NaBH_4$ hydrolysis reaction could be catalyzed via photocatalyst by the synergistical photo-thermal-catalysis.

2. Experimental

2.1. Materials

The reagents in this work were commercial reagents which without further purification. $Zn(CH_3COO)_2$, $Fe(NO_3)_3{\cdot}9H_2O$, $NaBH_4$, NaOH and D_2O were commercial analytical pure grade (99.9%, Aladdin Chemical Reagent Corp.). GeO_2 was commercial high purity grade (99.999%, Shanghai Macklin Biochemical Co., Ltd). Ethylenediamine was commercial analytical pure grade (99.5%, Sinopharm Chemical Reagent Corp.). Nitrogen (N_2), helium (He) were high pure grade (6 N, Yuanneng Biotechnology Co., Ltd.).

2.2. Preparation of photocatalysts

Zn_2GeO_4:***x***Fe^{3+} (***x*** = 0 to 0.10) catalysts were obtained by solvothermal method. In a typical synthesized, stoichiometric Zn $(CH_3COO)_2$ (1 mmol), GeO_2 and $Fe(NO_3)_3{\cdot}9H_2O$ were mixed with deionized water (3 mL) and ethylenediamine (6 mL) into a stainless autoclave. The aggregate amounts of Ge^{4+} ion and Fe^{3+} ion cations were 0.5 mmol. The mixture was stirring for one hour at 80 °C to form a homogeneous viscous colloid. Subsequently, the autoclave maintained at 180 °C for 10 h. Ultimately, the as-obtained precipitate was washed for several time with warm deionized water. The desired product was obtained after drying at 80 °C for several hours.

2.3. Characterization devices

Powder X-ray diffraction (XRD) data were obtained by a Philips PANanlytical X'Pert XRD system (Cu K*a* radiation, 45 kV, 40 mA, λ = 1.5418 Å). The morphologies of as-prepared catalyst were carried out by FEI Quanta 450FEG field emission scanning electron microscope system and JEM-2100F field emission transmission electron microscope system. The specific surface area was determined by using BET method on a Quantachrome Quadrasorb SI N_2 adsorption-desorption analyzer at 77 K. All the as-synthesized materials were degassed at 280 °C for 2 days. UV–Visible diffuse reflectance spectra (DRS) were measured by a Shimadzu UV-3600 UV–Vis-NIR spectrometer (λ = 200–800 nm) equipped with an integrating sphere. The background noise of the spectrometer was corrected by $BaSO_4$. Axis Ultra Imaging XPS Spectrometer was employed to obtain X-ray photoelectron spectroscopy spectrum.

2.4. Catalytic hydrogen evolution tests

The catalytic hydrogen evolution tests were performed in an evacuation AuLight CEL-PAEM-D8 photo-thermal characterization system. An online automatic Shimadzu GC-8A gas chromatograph equipped with GC-TCD (the carrier gas was N_2) and a 5A molecular sieve column was performed to detect the evolution amount of hydrogen. In a typical test, the as-prepared catalyst (20 mg), NaOH (1000 mg) and $NaBH_4$ (300 mg) were added into a three-neck Pyrex quartz glass vessel (150 mL). The reaction system kept vacuum for 20 min. Then, de-gased deionized (20 mL) water was injected into the glass vessel through the rubber plug by an injector. All the feed reactants were dispersed well by magnetically stirring. The temperature of the reactor vessel was maintained at the range of 10 to 40 °C by programmed-control system. UV-light and visible-light irradiation were provided by CEL-M500 mercury lamp (AuLight, 500 W) and CEL-LED100HA lamp (AuLight, 100 W), respectively.

3. Result and discussion

3.1. Characterization of catalysts

The XRD patterns of the as-obtained samples confirmed Zn_2GeO_4:***x***Fe^{3+} (x = 0 to 0.1) samples with fine crystallinity via solvothermal preparation method (See Fig. 1). The diffraction peaks of bare-Zn_2GeO_4 and low Fe^{3+} doped Zn_2GeO_4 (x = 0.01 to 0.05) samples were almost the same without any signal of impurity phase. However, it was quite obvious that there existed an impurity phase peak in the pattern of 10 atom% Fe^{3+}-doped Zn_2GeO_4. Zn_2GeO_4 is composed of two different tetrahedra (ZnO_4 and GeO_4) which bridged by O atoms with the space group of ***R***-3 (See the inset of Fig. 1). According to the data of ionic radius, the effective ionic radius of Fe^{3+} ion (0.49 Å) is smaller than Zn^{2+} ion (0.60 Å), but larger than Ge^{4+} ion (0.39 Å) in four-coordinated environment [26]. For the balance of electric charges, Fe^{3+} ion have to replace both Ge^{4+} ion and Zn^{2+} ion sites respectively, forming distorted molecular framework geometry. Therefore, the molecular framework of Zn_2GeO_4 could not tolerate a higher doping content of Fe^{3+} ion. The crystal parameters of Zn_2GeO_4:***x***Fe^{3+} (x = 0 to 0.05) samples were estimated by Rietveld refinement method and the minor error factors indicated reliable results (See Table S1 in the Supplementary material). It should be noticed that the value of a, c and V were expanded with doping concentration of Fe^{3+} ion, confirming the effective doping of Fe^{3+} ion into the Zn_2GeO_4 framework.

The morphologies of the as-obtained Zn_2GeO_4:***x***Fe^{3+} solid-solutions (x = 0 to 0.05) were observed via SEM measurements. Fig. 2 displayed that all the products exhibited flower-like morphology composed of nanobelts with 3–4 μm in length and several nanometers in width. The high resolution TEM images (See Fig. 3) presented distinct morphologies of Zn_2GeO_4 and Zn_2GeO_4:$0.05Fe^{3+}$, which confirmed the Zn_2GeO_4:***x***Fe^{3+} nanobelts with about 20 nm in width. Raul [27] et al. reported that the pH-value and GeO_2 content in the initial solution were relevant to the morphologies of Zn_2GeO_4. This work was not concerned about the morphology control of Zn_2GeO_4. As a typical sample, Zn_2GeO_4:$0.05Fe^{3+}$ was chosen for EDS analysis and element mapping investigation. The images demonstrated the atoms of Zn, Fe, Ge and O were homogeneous distributed on the surface of Zn_2GeO_4:$0.05Fe^{3+}$ (See Fig. 2).

The specific surface areas of the obtained Zn_2GeO_4:***x***Fe^{3+} (***x*** = 0 to 0.05) samples were measured by BET nitrogen absorption method. The BET plots (Fig. S1) demonstrated that the catalysts obtained via solvothermal method exhibited minor specific surface areas (2–3 $m^2{\cdot}g^{-1}$). The results were consistent with the observations from FESEM analyses.

To determine the chemical valence state of the ions in the as-obtained samples, X-ray photoelectron spectroscopy (XPS) was carried out on Zn_2GeO_4:$0.01Fe^{3+}$ as the representative of Zn_2GeO_4:***x***Fe^{3+} (***x*** = 0 to 0.05) samples (See Fig. 4). The high-resolution XPS revealed the characteristic binding energy peaks of Zn, Ge and Fe ions from the test sample (See the inset of Fig. 4). The characteristic peaks located at 1221.2 eV and 1252.4 eV were belonged to the orbits for Ge^{4+} ion (Ge $2\boldsymbol{p}_{1/2}$ and Ge $2\boldsymbol{p}_{3/2}$, respectively) [28]. Besides, the characteristic peaks of Zn^{2+} ions which located at 1045.6 eV (Zn $2\boldsymbol{p}_{1/2}$) and 1022.5 eV (Zn $2\boldsymbol{p}_{3/2}$), respectively [28]. In the right inset of Fig. 2, the two weak peaks

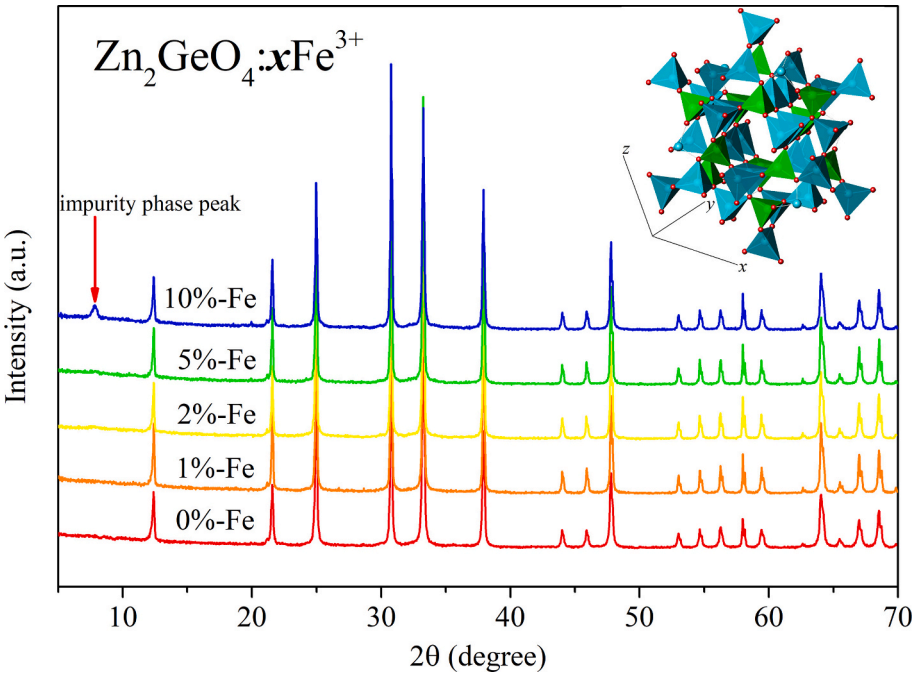

Fig. 1. The X-ray diffraction patterns of as-obtained Zn_2GeO_4:xFe^{3+} catalysts (x = 0 to 0.10). The impurity phase peak observed in the pattern of Zn_2GeO_4:0.10Fe^{3+}. (inset) The projection image of Zn_2GeO_4:xFe^{3+} exhibited through the [111] direction. Color code: cyan tetrahedra, ZnO_4; green tetrahedra, GeO_4; Cyan, green, red spheres represented Zn, Ge and O atoms, respectively.

appeared at 725.6 eV and 711.7 eV were corresponding to the orbits for Fe^{3+} ion (Fe 2$p_{1/2}$ and Fe 2$p_{3/2}$, respectively) [28]. Although the intensity of Fe 2p peaks were rather weak as the low concentration of Fe^{3+} ions, it still confirmed the effective doping of Fe^{3+} ion into the Zn_2GeO_4 framework.

The diffuse reflectance spectra in Fig. 5 revealed that the light adsorption of the Zn_2GeO_4:xFe^{3+} (x = 0 to 0.05) samples in the visible light region were remarkably enhanced with the Fe^{3+} ion doping into the framework of Zn_2GeO_4. Meanwhile, with the increasing concentration of Fe^{3+}, the spectra for Zn_2GeO_4:xFe^{3+} (x = 0 to 0.05) samples shifted toward the direction of long wave. The band gap energy of the Zn_2GeO_4:xFe^{3+} (x = 0.01 to 0.05) samples were calculated to be 3.81 eV to 3.40 eV from the Taus plots with the formula $\alpha h\nu = A(h\nu - E_g)^{n/2}$, in which E_g is the band gap energy, $h\nu$ is the incident photon energy, α is the absorption coefficient related to $h\nu$, and A is a constant [29]. The E_g of the Zn_2GeO_4:xFe^{3+} catalysts were much narrow than that of bare-$ZnGa_2O_4$ (4.52 eV) (See the inset of Fig. 5).

3.2. Catalytic performance

The investigations of catalytic H_2 evolution performance were carried out in three types of energy-driven conditions for each catalyst, such as thermal-driven, photo-driven and photo-thermal-driven. A mercury UV-light lamp was provided for bare-Zn_2GeO_4. Meanwhile, the LED visible-light lamp was provided for Zn_2GeO_4:xFe^{3+} (x = 0.01 to 0.05) solid-solutions. According to the Arrhenius formula $\ln k = \ln A - E_a/RT$, there exists an apparent positive linear correlation between the H_2 evolution rate and thermodynamic temperature. However, excessively high temperature is not suitable for practical hydrogen-energy application. Therefore, the temperature of thermal-driven and photo-thermal-driven condition were all 40 °C. The H_2 evolution rate for the as-prepared catalysts exhibited in Table 1. It was certainly manifested that the H_2 evolution rates for all the samples in photo-thermal-driven condition were several times than that in mono-energy-driven condition. Compared with Zn_2GeO_4:xFe^{3+} (x = 0.01 to 0.05) solid-solutions, Zn_2GeO_4 exhibited the highest catalytic performance for H_2 evolution (5.45 mmol·h^{-1}·g^{-1}) at 40 °C under UV-light irradiation. As Zn^{2+} and Ge^{4+} ions ensured the light harvest in the UV-light spectrum, the H_2 evolution rate for Zn_2GeO_4:xFe^{3+} (x = 0.01 to 0.05) solid-solutions decreased with the progresses of Fe^{3+} to Zn^{2+}/Ge^{4+} substitution. It should be noted that the H_2 evolution rate for Zn_2GeO_4:xFe^{3+} (x = 0.01 to 0.05) solid-solutions under visible light irradiation was greatly increased with the doping content of Fe^{3+} ions increasing. There was no doubt that Fe^{3+} ion improved the optical absorbance in the visible light region, which consistent with the observation in the DRS spectrum (See Fig. 5). Therefore, Zn_2GeO_4:0.05Fe^{3+} exhibited the maximum catalytic capacity (H_2: 2.93 mmol·h^{-1}·g^{-1}) at 40 °C under visible light irradiation. The results of the tests substantiated the synergistical photo-thermal-catalytic effect for Zn_2GeO_4:xFe^{3+} in $NaBH_4$ hydrolysis reaction.

3.3. Mechanism discussion

The photo-thermal-catalytic $NaBH_4$ hydrolyzation was the combination of $NaBH_4$ hydrolytic reaction and photocatalytic water splitting reaction. A set of reference experiments based on deuterium labeling method (H_2O in the reaction system was displaced by D_2O) were performed to verify the possible mechanism of the synergistically photo-thermal-catalytic effect. The experiments were catalyzed by bare-Zn_2GeO_4 (20 mg) under UV-light irradiation at 40 °C for two hours. Na_2-EDTA (10 mg), a conventional scavenger of photogenerated holes was added into the reference group A. Besides, the reference group B without Na_2-EDTA was treated as the control group. The composition analyses of the gaseous products were carried out by an online cryogenic gas chromatograph equipped with GC-TCD. The carrier gas was helium and operated at 77 K. Generally, the reactant with deuterium requires much higher apparent activation energy than the isostructural compounds with protium [30]. Therefore, the $NaBH_4$ hydrolytic reaction mainly released H_2. Meanwhile, the photocatalytic water splitting reaction released only D_2. The fingerprint peaks from gas chromatograph demonstrated that after the addition of Na_2-EDTA the proportions of protium (H_2) and deuterium (D_2) were decreased and increased, respectively (see Fig. S2). The reference experiments indicated that the consumption of photogenerated holes inhibited both $NaBH_4$ hydrolytic

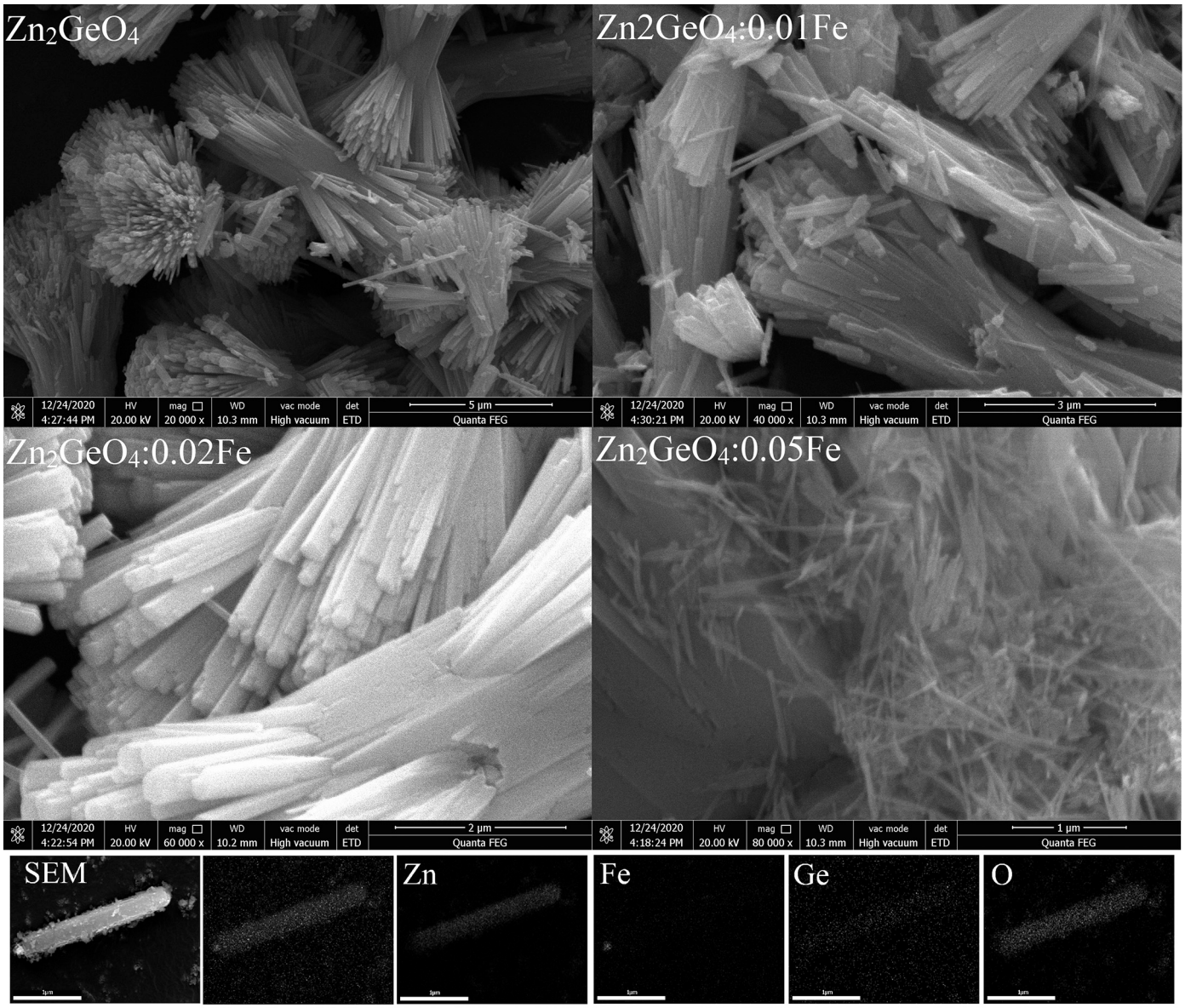

Fig. 2. FESEM images of Zn_2GeO_4, Zn_2GeO_4:0.01Fe^{3+}, Zn_2GeO_4:0.02Fe^{3+} and Zn_2GeO_4:0.05Fe^{3+}. SEM elemental mapping for Zn, Fe, Ge and O, the scale bars were 1 μm.

reaction and enhanced photocatalytic water splitting reaction. Consequently, the photogenerated holes served as a crucial role in the synergistically photo-thermal-catalytic effect. The process of the excess OH^- ions consumed by photogenerated holes could not only effectively enhanced the $NaBH_4$ hydrolysis reaction, but also inhibited the recombination of photogenerated e^-/h^+ pairs, leading much higher H_2 production for photocatalytic H_2 evolution process. Combined with the two factors above, hydrogen could be generated rapidly from $NaBH_4$ hydrolysis reaction under photo-thermal-driven condition. The probable reaction mechanism presented in the Graphic Abstract.

3.4. The kinetics studies of $NaBH_4$ hydrolytic reactions

For the kinetics study of the $NaBH_4$ hydrolytic reaction, the apparent activation energy ($\boldsymbol{E_a}$) is a major factor to evaluate the performance of catalyst. The studies were carried out under UV-light (bare-Zn_2GeO_4) and visible light irradiation (Zn_2GeO_4: 0.05Fe^{3+}), respectively. The hydrogen evolution rates increased significantly with temperature rising from 10 °C to 40 °C. (See Fig. S3a). The apparent activation energy is obtained by Arrhenius formula $\ln \boldsymbol{k} = \ln \boldsymbol{A} - \boldsymbol{E_a}/\boldsymbol{RT}$, in which $\boldsymbol{A}$ is a constant, $\boldsymbol{k}$ is the H_2 evolution rate, $\boldsymbol{R}$ is the universal molar gas constant and $\boldsymbol{T}$ is the thermodynamic temperature. The $\boldsymbol{E_a}$ values of bare-Zn_2GeO_4 (29.6 KJ·mol^{-1}) and Zn_2GeO_4: 0.05Fe^{3+} (33.7 KJ·mol^{-1}) for $NaBH_4$ hydrolytic reaction were calculated by the slop of the straight line on Arrhenius plot ($\ln \boldsymbol{k}$) versus temperature factor ($1/\boldsymbol{T}$) for each catalyst (See Fig. S3b). Obviously, a lower apparent activation energy for a catalyst means a better catalytic performance.

3.5. Stability tests

The structure and catalytic performance of catalysts should be stable and reliable in hot alkaline solution and irradiated with strong ultraviolet radiation. Zn_2GeO_4 (200 mg) as the catalyst for $NaBH_4$ hydrolytic reaction at 40 °C under ultraviolet irradiation for 10 h. After the reaction, the catalyst was recycled into the next round of testing with freshly prepared solution. The hydrogen evolution rate has witnessed slight downward trend in the inset of Fig. 6 due to the loss of catalyst in the recycled processes. At the end of the cycling tests, the powder XRD

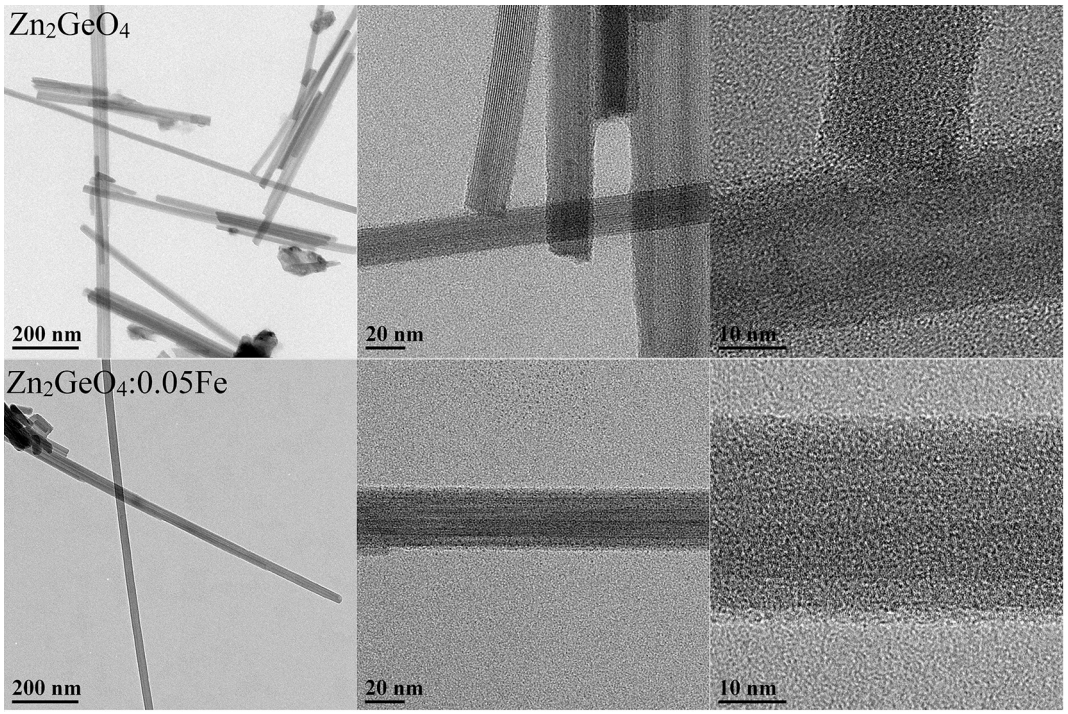

Fig. 3. TEM and HRTEM images of Zn_2GeO_4 and Zn_2GeO_4:0.05Fe^{3+}.

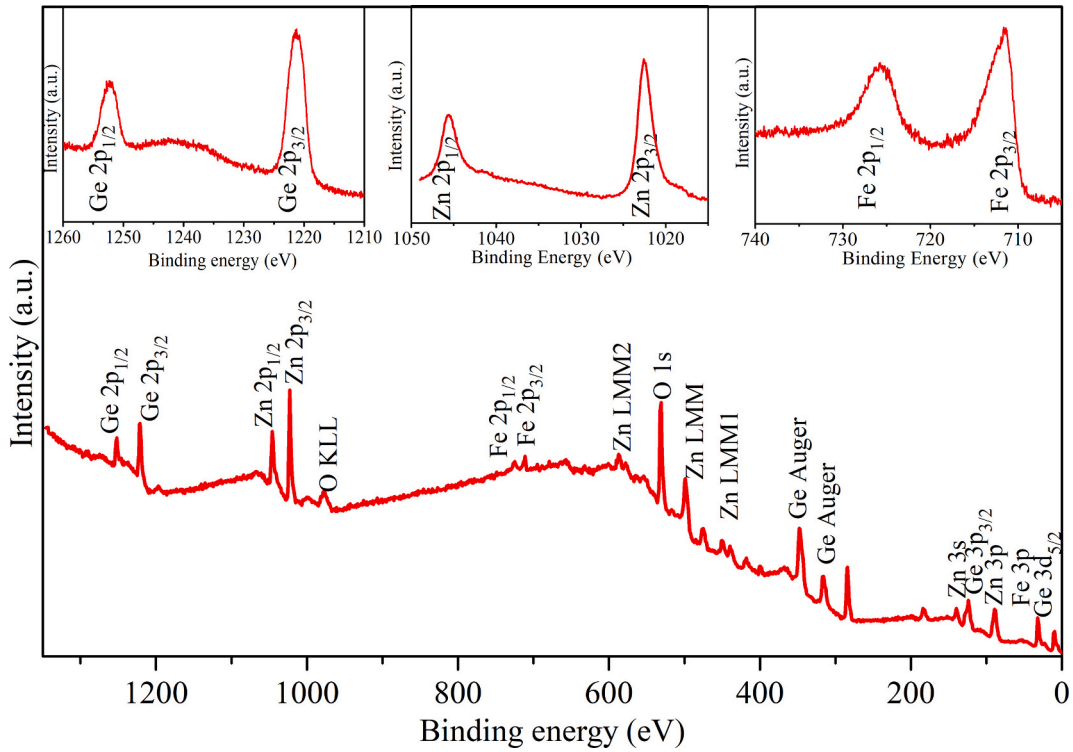

Fig. 4. The full survey X ray photoelectron spectroscopy spectra of Zn_2GeO_4:0.01Fe^{3+}. (inset) The high-resolution XPS spectra of each element in Zn_2GeO_4:0.01Fe^{3+} (Ge 2***p*** state, Zn-2***p*** state and Fe-2***p*** state).

pattern of Zn_2GeO_4 remained the same as the as-prepared sample without any impurity phase (see Fig. 6). Consequently, Zn_2GeO_4 could maintain its structure and provided reliable catalytic performance in harsh photo-thermal-driven condition for $NaBH_4$ hydrolytic reaction.

4. Conclusions

In the present work, Zn_2GeO_4:***x***Fe^{3+} (***x*** = 0 to 0.05) samples were successfully synthesized via a simple solvothermal method. The as-obtained photocatalysts were applying to H_2 evolution from $NaBH_4$ hydrolysis reaction. The process of the excess OH- ions consumed by

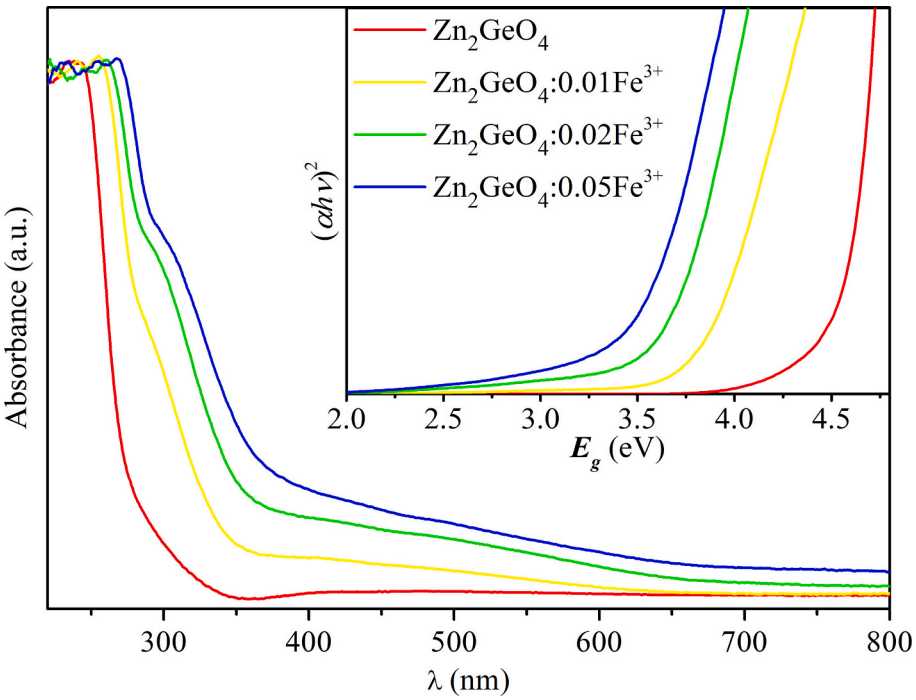

Fig. 5. Diffuse reflectance spectra for Zn_2GeO_4:$x$$Fe^{3+}$ (x = 0 to 0.05) samples. (inset) Tauc plot for Zn_2GeO_4:$x$$Fe^{3+}$ (x = 0 to 0.05) samples.

Table 1
The H_2 evolution kinetics of $NaBH_4$ hydrolysis reaction catalyzed via Zn_2GeO_4:$x$$Fe^{3+}$ (x = 0 to 0.05) in the various types of energy-driven conditions.

	40 °C in dark	10 °C & UV-light	40 °C & UV-light	10 °C & visible light	40 °C & visible light
Zn_2GeO_4	119.33	442.56	5447.55	–	–
Zn_2GeO_4:0.01Fe^{3+}	125.15	423.28	4883.34	61.59	400.75
Zn_2GeO_4:0.02Fe^{3+}	131.20	408.37	4644.28	130.44	1419.71
Zn_2GeO_4:0.05Fe^{3+}	141.58	392.56	4245.19	254.78	2927.99

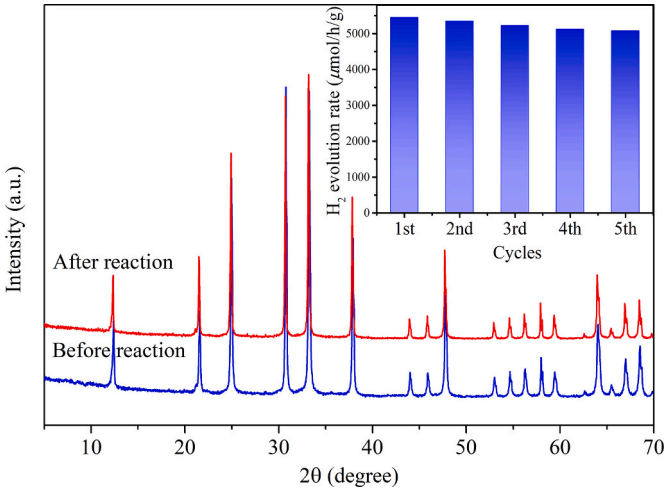

Fig. 6. The XRD patterns of bare-Zn_2GeO_4 before and after reaction. (inset) The H_2 evolution rate for Zn_2GeO_4 in $NaBH_4$ hydrolytic reaction to cycling tests.

photogenerated holes could not only effectively enhanced the $NaBH_4$ hydrolysis reaction, but also inhibited the recombination of photogenerated e^-/h^+ pairs, leading much higher H_2 production for photocatalytic H_2 evolution process. The as-prepared catalysts exhibited remarkable photo-thermal synergism, the H_2 evolution rate in photo-thermal-driven condition was several times higher than that in mono-energy driven condition. This work demonstrated that the conventional photocatalyst could be used as the highly efficient H_2 evolution catalyst for $NaBH_4$ hydrolysis reaction via the synergistically photo-thermal-catalytic effect.

Declaration of Competing Interest

The authors declare that they have no known competing financial interests or personal relationships that could have appeared to influence the work reported in this paper.

Acknowledgements

This work was supported by National Natural Science Foundation of China (Grants number 21808076); Natural Science Foundation of Jiangsu Province, China (Grants number BK20181069); Natural Science Foundation of the Jiangsu Higher Education Institutions of China (20KJB430050); Huai'an Municipal Science and Technology Bureau (HAB201907).

Appendix A. Supplementary data

Supplementary data to this article can be found online at https://doi.org/10.1016/j.catcom.2021.106321.

References

[1] Jun Yang, Andrea Sudik, Christopher Wolverton, Donald J. Siegel, High capacity hydrogen storage materials: attributes for automotive applications and techniques for materials discovery, Chem. Soc. Rev. (39) (2010) 656–675.
[2] Hazel Reardon, James M. Hanlon, Robert W. Hughes, Agata Godula-Jopek, Tapas K. Mandala, Duncan H. Gregory, Emerging concepts in solid-state hydrogen storage: the role of nanomaterials design, Energy Environ. Sci. (5) (2012) 5951–5979.
[3] Naoki Ishida, Yoshiki Kamae, Keigo Ishizu, Yuka Kamino, Hiroshi Naruse, Masahiro Murakami, Sustainable system for hydrogenation exploiting energy derived from solar light, J. Am. Chem. Soc. (143) (2021) 2217–2220.
[4] Yoshitsugu Kojima, Hydrogen storage materials for hydrogen and energy carriers, Int. J. Hydrogen Energ. 44 (2019) 18179–18192.

[5] Yongyang Zhu, Liuzhang Ouyang, Hao Zhong, Jiangwen Liu, Hui Wang, Huaiyu Shao, Zhenguo Huang, Min Zhu, Closing the loop for hydrogen storage: facile regeneration of $NaBH_4$ from its hydrolytic product, Angew. Chem. Int. Edit. (59) (2020) 8623–8629.
[6] Mark Paskevicius, Lars H. Jepsen, Pascal Schouwink, Radovan Černý, Dorthe B. Ravnsbæk, Yaroslav Filinchuk, Martin Dornheim, Flemming Besenbacher, Torben R. Jensen, Metal borohydrides and derivatives-synthesis, structure and properties, Chem. Soc. Rev. (46) (2017) 1565–1634.
[7] Yan Wang, Guode Li, Shiwei Wu, Yongsheng Wei, Wei Meng, Yuan Xie, Ying Cui, Xin Lian, Yongge Chen, Xinyu Zhang, Hydrogen generation from alkaline NaBH4 solution using nanostructured Co-Ni-P catalysts, Int. J. Hydrogen Energ. (42) (2017) 16529–16537.
[8] Changli Peng, Tianshuo Li, Yongjin Zou, Cuili Xiang, Fen Xu, Jian Zhang, Lixian Sun, Bacterial cellulose derived carbon as a support for catalytically active Co-B alloy for hydrolysis of sodium borohydride, Int. J. Hydrogen Energ. (46) (2021) 666–675.
[9] Umit B. Demirci, Philippe Miele, Cobalt in $NaBH_4$ hydrolysis, Phys. Chem. Chem. Phys. (12) (2010) 14651–14665.
[10] Hao Zhang, Tao Ling, Du Xiwen, Gas-phase cation exchange toward porous single-crystal CoO nanorods for catalytic hydrogen production, Chem. Mater. (27) (2015) 352–357.
[11] Xi Zhao, Dongyan Xu, Kai Liu, Ping Dai, Jun Gao, Remarkable enhancement of PdAg/rGO catalyst activity for formic acid dehydrogenation by facile boron-doping through $NaBH_4$ reduction, Appl. Surf. Sci. (512) (2020), 145746.
[12] Yingbo Chen, Hern Kim, Ni/Ag/silica nanocomposite catalysts for hydrogen generation from hydrolysis of NaBH4 solution, Mater. Lett. (62) (2008) 1451–1454.
[13] Fan Yang, Kui Cheng, Ke Ye, Xiaopei Wei, Xiao Xue, Fen Guo, Guiling Wang, Dianxue Cao, High performance of Au nanothorns supported on Ni foam substrate as the catalyst for $NaBH_4$ electrooxidation, Electrochim. Acta (115) (2014) 311–316.
[14] Hongming Zhang, Zhang Lu, Ismael A. Rodríguez-Pérez, Wenkang Miao, Kangli Chen, Wenfeng Wang, Yuan Li, Shumin Han, Carbon nanospheres supported bimetallic Pt-Co as an efficient catalyst for $NaBH_4$ hydrolysis, Appl. Surf. Sci. (540) (2021), 148296.
[15] Betül Şen, Esma Hazal Akdere, Aysun Şavk, Emine Gültekin, Özge Paralı, Haydar Göksu, Fatih Şena, A novel thiocarbamide functionalized graphene oxide supported bimetallic monodisperse Rh-Pt solid-solutions (RhPt/TC@GO NPs) for Knoevenagel condensation of aryl aldehydes together with malononitrile, Appl. Catal. B (225) (2018) 148–153.
[16] Nurettin Sahiner, Ozgur Ozay, Erk Inger, Nahit Aktas, Controllable hydrogen generation by use smart hydrogel reactor containing Ru nano catalyst and magnetic iron solid-solutions, J. Power Sources (196) (2011) 10105–10111.
[17] Divya Prasad, Komal N. Patil, N. Sandhya, C.R. Chaitra, Jayesh T. Bhanushali, Akshaya K. Samal, Rangappa S. Keri, Arvind H. Jadhav, Bhari Mallanna Nagaraja, Highly efficient hydrogen production by hydrolysis of $NaBH_4$ using eminently competent recyclable Fe_2O_3 decorated oxidized MWCNTs robust catalyst, Appl. Surf. Sci. (489) (2019) 538–551.
[18] Changwoo Kim, Seung Soo Lee, Wenlu Li, John D. Fortner, Towards optimizing cobalt based metal oxide nanocrystals for hydrogen generation via $NaBH_4$ hydrolysis, Appl. Catal. A (589) (2020), 117303.
[19] Jingya Guo, Benzhi Wang, Dandan Yang, Zixia Wan, Puxuan Yan, Jianniao Tian, Tayirjan Taylor Isimjan, Xiulin Yang, Iron-doped Rugae-like Ni_2P-CoP nanoarrays as a bi-functional catalyst for hydrogen generation: $NaBH_4$ hydrolysis and water reduction, Appl. Catal. B (265) (2020), 118584.
[20] Mark Paskevicius, Lars H. Jepsen, Pascal Schouwink, Radovan Černý, Dorthe B. Ravnsbæk, Yaroslav Filinchuk, Martin Dornheim, Flemming Besenbacher, Torben R. Jensen, Metal borohydrides and derivatives-synthesis, structure and properties, Chem. Soc. Rev. (46) (2017) 1565–1634.
[21] Yongsheng Wei, Maosen Wang, Fu Wenying, Wei Lu, Xinsheng Zhao, Xiangyang Zhou, Meng Ni, Haijiang Wang, Highly active and durable catalyst for hydrogen generation by the $NaBH_4$ hydrolysis reaction: CoWB/NF nanodendrite with an acicular array structure, J. Alloy Compd. (836) (2020) 155429.
[22] Shuo Hou, Zhiquan Wei, Xiaocheng Dai, Minghui Huang, Fangxing Xiao, General layer-by-layer assembly of multilayered photoanodes: triggering Tandem charge transport toward photoelectrochemical water oxidation, Inorg. Chem. (59) (2020) 7325–7334.
[23] Yubing Li, Tao Li, Xiaocheng Dai, Minghui Huang, Shuo Hou, Fu Xiaoyan, Zhiquan Wei, Yunhui He, Guangcan Xiao, Fangxing Xiao, Precese tuning of coordination positions for transition-metal ions via layer-by-layer assembly to enhance solar hydrogen production, ACS Appl. Mater. Interfaces (12) (2020) 4373–4384.
[24] Fu Xiaoyan, Zhiquan Wei, Shuai Xu, Xin Lin, Shuo Hou, Fangxing Xiao, Maneuvering intrinsic instability of metal nanoclusters for boosted solar-powered hydrogen production, J. Phys. Chem. Lett. (11) (2020) 9138–9143.
[25] Qiaoqi Li, Lili Zhang, Chao Tang, Pusu Zhao, Chengzhu Yin, Jingzhou Yin, Synthesis of $Zn(In_xGa_{1-x})_2O_4$ solid-solutions with tunable band-gaps for enhanced photocatalytic hydrogen evolution under solar-light irradiation, Int. J. Hydrogen Energ. (45) (2020) 6621–6628.
[26] Robert D. Shannon, Revised effective ionic radii and systematic studies of interatomic distances in halides and chalcogenides, Acta Crystallogr. Sect. A 32 (1976) 751–767.
[27] Venkata Bharat Ram Boppana, Nathan D. Hould, Raul F. Lobo, Synthesis, characterization and photocatalytic properties of novel zinc germanate nano-materials, J. Solid State Chem. (184) (2011) 1054–1062.
[28] J.F. Moulder, William F. Stickle, Peter Sobol, Kenneth D. Bomben, Handbook of X-ray Photoelectron Spectroscopy, Perkin-Elmer Corporation, Eden Prairie, MN, 1992.
[29] Qiaoqi Li, Lili Zhang, Chao Tang, Jingzhou Yin, Preparation of $Zn(Fe_xGa_{1-x})_2O_4$ solid solutions as photocatalyst for CO_2 reduction under simulated solar-light irradiation, Eur. J. Inorg. Chem. 30 (2019) 3476–3480.
[30] Jaemoon Yang, Deuterium, Discovery and Applications in Organic Chemistry, 2016, pp. 5–18.